Comparative study of single-layer, bilayer, and trilayer mirrors with enhanced x-ray reflectance in 0.5- to 8-keV energy region

Yang Yang,[a] Qiushi Huang,[a,*] Igor V. Kozhevnikov,[b] Yingyu Liao,[a] Runze Qi,[a] Andrey A. Sokolov,[c] Zhuangzhuang Zhang,[a] Zhong Zhang,[a] and Zhanshan Wang[a,*]

[a]Tongji University, Institute of Precision Optical Engineering, School of Physics Science and Engineering, Key Laboratory of Advanced Micro-Structured Materials MOE, Shanghai, China
[b]Russian Academy of Sciences, Federal Scientific Research Centre "Crystallography and Photonic," Shubnikov Institute of Crystallography, Moscow, Russia
[c]Helmholtz-Zentrum Berlin für Materialien und Energie, BESSY-II, Berlin, Germany

Abstract. Effective area is one of the most important parameters of x-ray telescopes. It can be increased by enlarging the entrance aperture or maximizing the reflectivity through the proper designing and optimization of the reflecting coating. A method to increase the reflectivity of grazing incidence x-ray mirrors in the 0.5- to 8-keV energy region is analyzed. The idea consists in the use of a trilayer reflecting coating instead of single-layer one (e.g., C/Ni/Pt mirror instead of Pt one). Deposition of low-absorbing medium-Z and low-Z layers onto the top of strongly absorbing high-Z material results in essential increase in the reflectivity while keeping the same width of the reflectivity plateau. In particular, C/Ni/Pt trilayer mirror demonstrates enhancement of the double reflection coefficient by a factor achieving 1.5 to 3.5 compared to that of Pt-coated mirror. The effective area of a telescope is also considerably increased. The experimental results are in a very good agreement with the theoretical predictions. In addition, the C/Ni/Pt trilayer mirror exhibits a reasonable thermal stability and a relatively low compressive stress of about −550 MPa. © *The Authors. Published by SPIE under a Creative Commons Attribution 4.0 Unported License. Distribution or reproduction of this work in whole or in part requires full attribution of the original publication, including its DOI.* [DOI: 10.1117/1.JATIS.6.4.044001]

Keywords: x-ray telescope; grazing incidence reflection; bilayer and trilayer mirrors.

Paper 20050 received May 21, 2020; accepted for publication Sep. 22, 2020; published online Oct. 8, 2020.

1 Introduction

Advancements in x-ray space astronomy are essentially based on progressive increases in the performance of x-ray telescopes' effective area, angular resolution, and field of view.[1–3] The effective area characterizes the ability of a telescope to collect incident radiation. It is determined by the geometrical size of the open entrance aperture and the reflectance of the telescope mirrors. As an example, technical specifications for several modern x-ray telescopes that are currently in operation, Chandra, XMM-Newton, and NuSTAR, are given below. The Chandra telescope[4] achieves an ultrahigh angular resolution of 0.5 arc sec with a relatively low effective area of 800 cm^2 at 1 keV. The XMM-Newton telescope[5] has a larger effective area of 1400 cm^2 at 1 keV and a moderate angular resolution of 15 arc sec. The NuSTAR telescope[6] is characterized by an essentially lower angular resolution of 58 arc sec; however, it has an extremely large effective area of 2400 cm^2. The Athena telescope,[7] which is under development for launch in ∼2030, will have an unprecedented effective area of 14,000 cm^2 at 1 keV.

Two missions, the Einstein Probe[8,9] (EP) and the Enhanced X-ray Timing and Polarimetry[10] (eXTP), were recently proposed in China. The goal of these missions is to study matter under the conditions of extreme density, gravity, and magnetism as well as faint flashes of x-rays produced by highly energetic cosmic events. The telescopes are planned for operation in the energy range

*Address all correspondence to Qiushi Huang, E-mail: huangqs@tongji.edu.cn; Zhanshan Wang, E-mail: wangzs@tongji.edu.cn

of 0.5 to 4 keV and 0.5 to 10 keV, respectively, in the grazing incidence geometry so that the grazing incidence angle is varied within 0.3 deg to 0.9 deg interval for the EP mission and within 0.15 deg to 0.7 deg interval for the eXTP mission. Because of very hard requirements imposed on the telescope mass and size, a reasonable way to enhance the effective area and thus the telescope sensitivity is to increase the reflectivity of the telescope mirrors.

In this paper, we performed a comparative study of the reflectivity from single-layer, bilayer, and trilayer grazing incidence mirrors to optimize the effective area within the 0.5-to 8-keV spectral interval. In Sec. 2, we consider the physical phenomena that allow a substantial increase in the grazing incidence reflectivity and discuss the design of optimal bi- and trilayer structures. In Sec. 3, we describe the experimental results on the study of the single-layer, bilayer, and trilayer mirrors, which are in a good agreement with the theoretical predictions.

2 Design of Grazing Incidence Mirrors

A single-layer reflective coating is typically used for telescope mirrors operating at photon energies below 10 keV. As a rule, heavy (high-Z) materials, such as iridium, gold, or platinum, are chosen as mirror coatings to broaden the total external reflection (TER) region and extend the spectral bandpass of a telescope. For instance, a single Ir layer is used in the Chandra telescope[4] to achieve high reflectivity within the 0.1- to 10-keV energy range. Similarly, a single reflective gold coating was chosen for the XMM-Newton telescope[11] to extend the energy bandwidth up to 7 keV.

The double-reflection coefficients R^2 for different coatings in a Wolter-type telescope are given in Fig. 1 in the energy range of 0.5 to 10 keV and at a grazing incident angle of 0.5 deg, the value being taken for definiteness as the mean value of the grazing angle in the EP and eXTP telescopes. The calculations were carried out using bulk density of the mirror materials, the optical constants being taken from the Centre for X-Ray Optics (CXRO) database.[12] The interlayer as well as the interfacial roughness were neglected when mirror designing, whereas they were taken into account when analyzing experimental data in Sec. 3. The interlayer was assumed in Sec. 3 to be described by the error function so that its amplitude reflectivity is given by the Nevot–Croce formula.[13] Notice that the polarization dependence of the reflectivity at small grazing angles $\theta < 1$ deg is so small that it is impossible to distinguish in the graph among the reflectivity curves calculated for different polarizations of the incident beam.

Figure 1 demonstrates two main shortcomings of coatings using high-Z reflecting materials. First, there is a deep minimum in the reflectivity curve at ~2 keV related to the M-edge absorption. Second, the coefficient R^2 near the absorption edge is relatively low (~50% to 60% after a

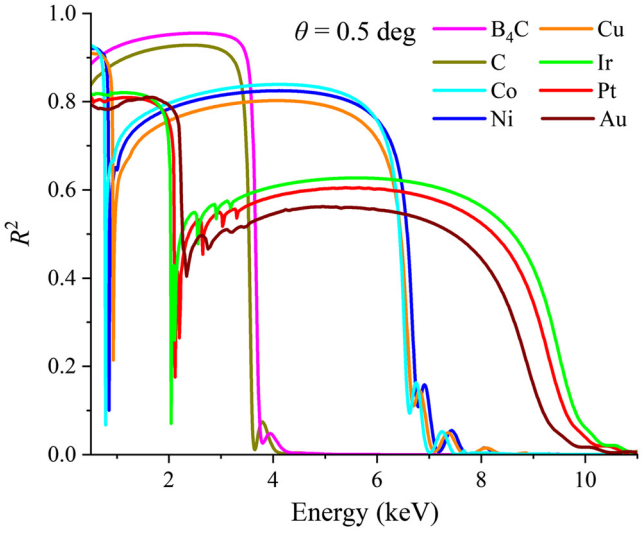

Fig. 1 Double-reflection coefficient R^2 of several bulk materials as a function of the photon energy for a fixed grazing incidence angle of $\theta = 0.5$ deg.

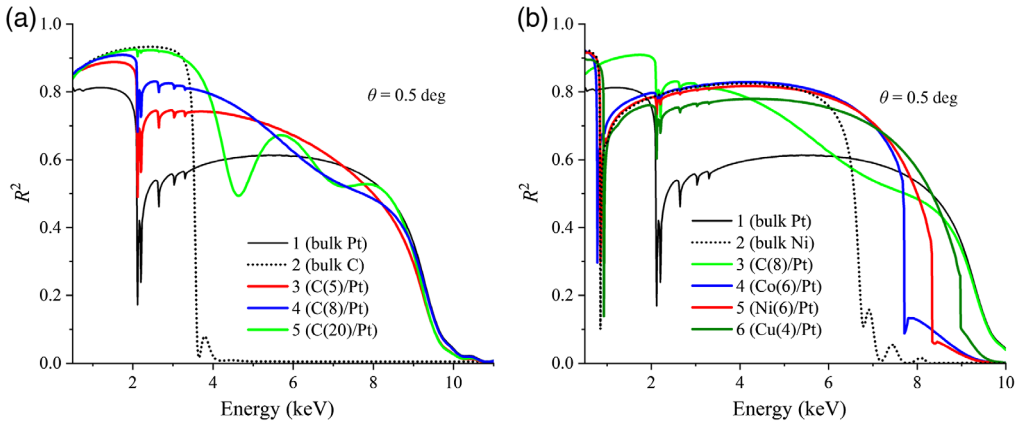

Fig. 2 (a) Coefficient R^2 of C/Pt bilayer mirrors versus the photon energy at a fixed grazing incidence angle $\theta = 0.5$ deg. (b) Coefficient R^2 of bilayer mirrors with different medium-Z materials . The numbers in parentheses indicate the thickness of the upper layer in nm. The thickness of the Pt layer was set to 50 nm. For comparison, the R2 coefficients for bulk Pt, Ni, and C are also shown.

double reflection) because of the high absorptivity of heavy materials in the energy range above the absorption edge.

To address these problems, many authors have suggested covering heavy materials with a thin layer of a low-Z material, such as C or B_4C[14–17] or even an organic compound (polyethylene[18]). As shown in Fig. 1, the low x-ray absorption by C and B_4C contributes to an extremely high R^2 coefficient of over 95% at 2 keV. Although the reflectivity plateau is much narrower than that of high-Z materials, it covers their absorption M-edges. Therefore, deposition of a low-Z material on top of a high-Z material could increase reflectivity at low photon energies and mask the deep minimum in the reflectivity curve.

The R^2 coefficient for the C/Pt bilayer is shown in Fig. 2(a) along with the R^2 coefficients for bulk Pt and C for comparison. As demonstrated, a deposition of a 5-nm-thick C layer on top of a Pt layer (curve 3) significantly increased the R^2 coefficient of the C/Pt bilayer compared to that of bulk Pt. Note that the reflectivity of bulk carbon is high at $E < 3$ keV only (after double reflection), although the effect of the C layer is observed up to $E \sim 7$ keV. This fact is explained by the positive interference of waves reflected from the C layer interfaces outside of the TER region of the carbon. Increasing the thickness of the carbon layer to 8 nm (curve 4) contributes to a further enhancement in the R^2 coefficient at $E < 5$ keV and the masking of the M-edge of absorption of platinum, at the cost of lower R^2 coefficient at $E > 5$ keV due to the negative interference of the reflected waves. If the C layer thickness is increased to 20 nm (curve 5), the interference oscillations become more pronounced. As a result, an overly thick carbon layer is poorly suited for a practical design despite the extremely high reflectivity of the C/Pt bilayer at $E < 3$ keV. Thus we concluded that deposition of a thin C layer on top of a Pt layer could increase the reflectivity owing to the effect of TER from the C layer at $E < 3$ keV and positive interference of the waves reflected from the C film interfaces outside of the TER region. However, the coefficient R^2 could be improved significantly only at $E < 6$ keV (for $\theta = 0.5$ deg).

Therefore, we next consider mirrors that consist of a thin layer of a medium-Z material (Co, Ni, or Cu) deposited on the top of a Pt layer. Figure 1 demonstrates that these materials with a relatively low absorptivity are characterized by a higher coefficient R^2 than that of high-Z materials at $E < 6$ keV. The reflectivity plateau of medium-Z materials is two times wider compared to that of low-Z materials. The R^2 coefficients of Pt-based bilayers and, for comparison, those of bulk Pt and Ni, are shown in Fig. 2(b). It can be seen that the coefficient R^2 of a Ni/Pt mirror (curve 5) is practically the same as that of bulk Ni (curve 2) for $E < 6$ keV (within the TER region of Ni). Furthermore, it is higher than the coefficient R^2 of bulk Pt (curve 1) for photon energies up to ~8 keV owing to the positive interference of the reflected waves. A sharp decrease in the Ni/Pt coefficient R^2 at E ~ 8.4 keV is related to the K-edge in Ni absorption. Note that the coefficient R^2 of the Ni/Pt bilayer is higher than that of the C/Pt bilayer within the photon energy range $E = 2$ to 8 keV.

Similarly, Co/Pt and Cu/Pt bilayers [curves 4 and 6 in Fig. 2(b)] exhibit a sharp coefficient R^2 decrease at $E \sim 7.7$ and 9 keV caused by the K-edge of absorption of Co and Cu, respectively. In the calculations, we applied a 4-nm-thick Cu layer, thinner than the Co and Ni layers (6 nm), to increase the Cu/Pt mirror reflectivity at $E > 8$ keV. This configuration is important for the eXTP telescope to achieve a wider reflectivity bandpass. A further decrease in the Cu layer thickness would result in curve 6 (Cu/Pt) approaching curve 1 (bulk Pt).

The use of an intermediate material with a smaller Z is unacceptable for our goal owing to the shift in the absorption edge to a lower energy. The use of intermediate materials with a larger Z (e.g., Zn, Ga, and Ge) is also problematic because their polarizability is lower than that of Ni owing to their lower density, and the width of the reflectivity plateau is therefore essentially decreased. Moreover, there are no examples of using these materials in the area of x-ray optics.

After putting a 6-nm-thick Ni or Co film on a Pt layer, the sharp minimum in reflectivity at $E \sim 2$ keV is essentially removed. However, another deep minimum arises at $E \sim 0.7$ to 1 keV, which is related to the L-edge absorption of the intermediate materials. As described above, this minimum can be masked using an additional thin layer of low-Z material. Thus to obtain mirrors with high reflectivity in the whole target range, we should consider trilayer reflective coatings.[19]

Based on the analysis of x-ray reflection from bilayer mirrors (Fig. 2), we can specify the optimization procedure of trilayer mirror. On the one hand, the thickness of low-Z and medium-Z layers should be large enough to provide high reflectivity in the TER region and to mask absorption edge of the underlying layer. On the other hand the thickness should not be too large to prevent appearance of interference oscillations on the reflectivity curve. The results of calculations (Fig. 2) demonstrate that the thickness of low-Z and medium-Z layers should lie in the 3- to 8-nm interval. The final choice of layer materials is based on additional considerations discussed below.

The coefficient R^2 of trilayer C/Ni/Pt mirrors as a function of the photon energy for a fixed grazing incidence angle $\theta = 0.5$ deg is plotted in Fig. 3(a). For comparison, the coefficient R^2 of the C/Pt and Ni/Pt bilayers, as well as that of the bulk Pt, is also presented. The coefficient R^2 of the trilayer mirrors (curves 4 to 6) significantly exceeds that of the C/Pt bilayer within the energy range $E = 2$ to 8 keV and is higher than the coefficient R^2 of the Ni/Pt bilayer at $E < 2$ keV. A moderate decrease in coefficient R^2 compared to that of the Ni/Pt bilayer is observed at $E \sim 6$ to 7 keV when the C layer thickness is 8 nm (curves 4 and 5). A decrease in thickness to 5 nm can be used to partially overcome this shortcoming, although at the cost of a decrease in the coefficient R^2 at $E < 4$ keV. A decrease in the Ni layer thickness from 6 nm (curve 4) to 3 nm (curve 5) does not change the coefficient R^2 at $E < 8$ keV, but results in its substantial enhancement (by several times) at $E > 8.4$ eV, which is important if the operation range is to be widened up to 10 keV for the eXTP telescope.

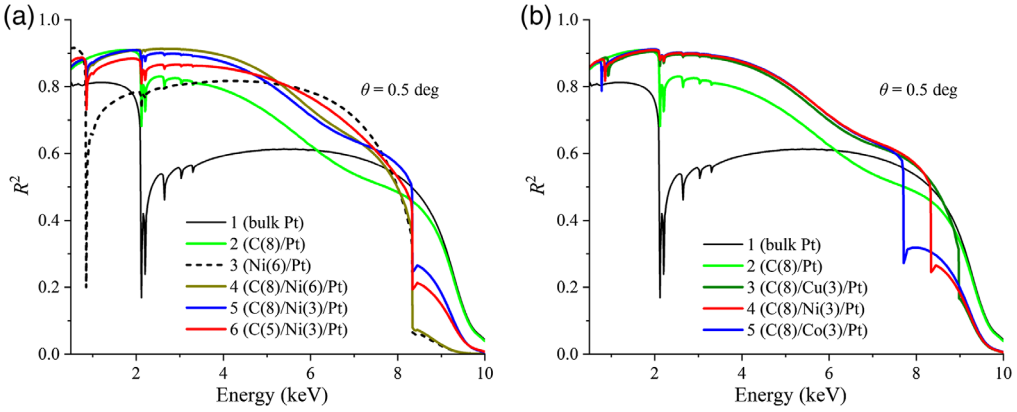

Fig. 3 (a) Coefficient R^2 of C/Ni/Pt trilayer mirrors versus the photon energy at a fixed grazing incidence angle $\theta = 0.5$ deg. (b) Coefficient R^2 of trilayer mirrors with different intermediate materials. The numbers in parentheses indicate the layer thickness in nm. The thickness of the Pt layer was set to 50 nm. For comparison, the coefficient R^2 of bulk Pt and the C/Pt and Ni/Pt bilayers is also shown.

The final design of the C/Ni/Pt trilayer coating can be chosen based on these considerations rather than on a value of the reflectivity integrated over energy. Indeed, the integrated reflectivity is practically the same for all trilayer mirrors presented in Fig. 3(a).

Figure 3(b) illustrates the coefficient R^2 of trilayer mirrors with different intermediate materials (Co, Ni, and Cu). The coefficient R^2 is almost the same at photon energies below that of the K-edge of the absorption, whereas the width of the spectral interval of the operation is largest for the Cu-containing trilayer. Although copper was also used in the fabrication of thin-film coatings,[20] including multilayer structures for x-ray optics,[21] the deposition technology of Ni has been more extensively developed to date than that of Cu.

So far, our discussion of the spectral dependence of the reflectivity was limited to a fixed grazing incidence angle $\theta = 0.5$ deg. Figure 4 presents the changes in coefficient R^2 with the grazing incidence angle varying from 0.3 deg to 0.9 deg. Short-scale oscillations observed in the reflectivity curve of a Pt mirror within the 2.1- to 3.2-keV energy range are independent from the interference effect; they are caused by quasiperiodic variations in the Pt polarizability near the absorption edge and their position on the energy axis is not dependent on the incident angle.

It can be seen from Fig. 4 that the conclusion made above for $\theta = 0.5$ deg is valid for other grazing incidence angles: the C/Ni/Pt trilayer demonstrates a higher reflectance compared to that of Pt and C/Pt mirrors. The reflectivity enhancement is highest at large grazing angles. Here the Ni layer thickness in the Ni/Pt bilayer (curve 3 in Fig. 4) differs from that in Fig. 3 to be consistent with other samples in Fig. 4. In particular, for incident angles 0.5 deg to 0.9 deg, the reflectivity of the C/Ni/Pt trilayer in the 2- to 4-keV range is higher than that of the Pt-coated mirror by a factor of 1.5 to 3.5.

We can now apply the developed approach to an analysis of the ultimate efficiency of a telescope[22] that consists of two co-aligned conical moduli approximating the hyperboloid and paraboloid sections of a Wolter type-I reflector. In the design of the telescope, we used 66 nested

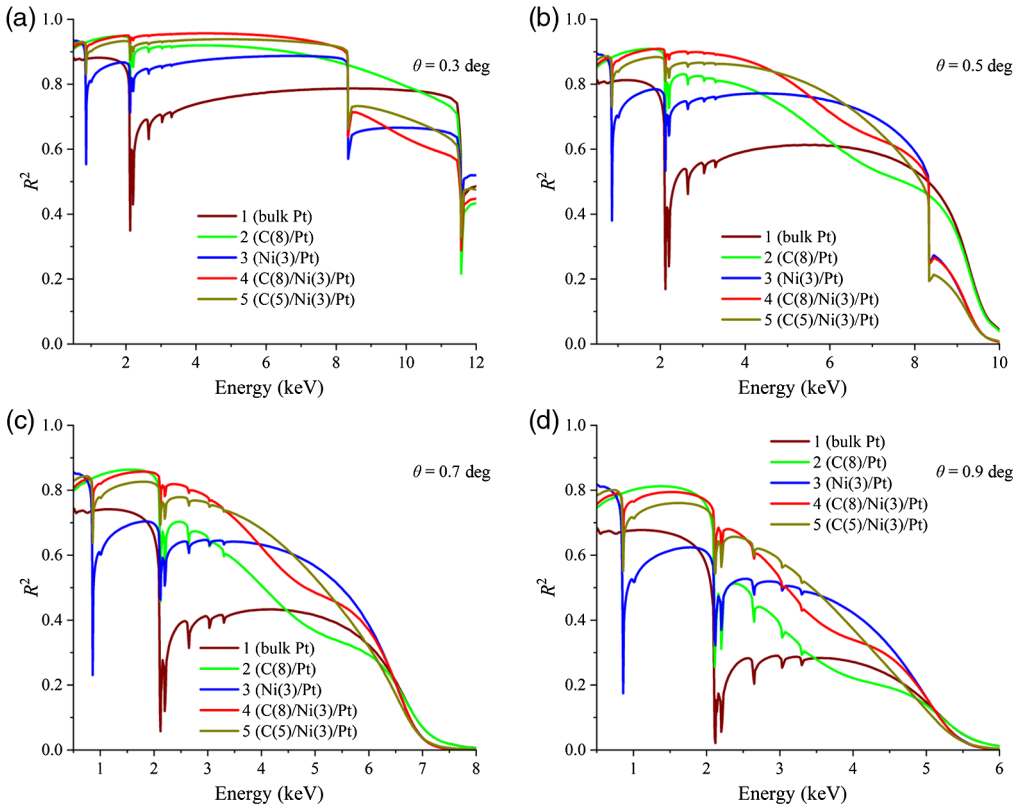

Fig. 4 Coefficient R^2 of C/Ni/Pt trilayer mirrors versus the photon energy at different grazing angles θ, (a) $\theta = 0.3$ deg, (b) $\theta = 0.5$ deg, (c) $\theta = 0.7$ deg, and (d) $\theta = 0.3$ deg. The coefficient R^2 plots for bulk Pt and the C/Pt and Ni/Pt bilayers are also shown for comparison. The numbers in parentheses indicate the layer thickness in nm. The thickness of the Pt layer was set to 50 nm.

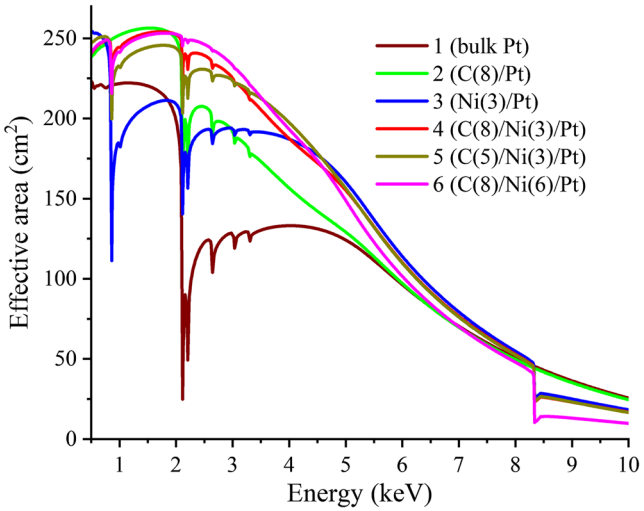

Fig. 5 Comparison of ray-tracing simulations of effective area using different reflecting coatings.

glass shells that had the length of 100 mm and the thickness of 0.3 mm. The grazing angle of x-rays propagating along the optical axis varies from 0.29 deg to 0.89 deg. The entrance aperture of the telescope is a concentric annulus with a 250-mm outer diameter and an 80-mm inner diameter. The focal length of the telescope is 2000 mm, and the open geometrical aperture is 300 cm^2.

Using a ray-tracing program, we compared the effective area of the telescope when using different reflective coatings. The results are shown in Fig. 5. As in the above considerations, increasing the number of layers in a reflective coating progressively results in the enhancement of the effective area. The effective area is improved significantly using the C/Ni/Pt trilayer coating; namely, it is increased by a factor of 1.5 to 2.5 in the 2- to 4-keV range compared to the mirror coated with a single Pt layer. By varying the thickness of the C and Ni layers (curves 4 to 6), we can slightly increase the effective area for a particular photon energy range, albeit at the cost of a corresponding decrease in another spectral range.

3 Experimental Results and Discussion

For the experimental study, we chose a Pt (10 nm) single layer, a C (8 nm)/Pt (10 nm) bilayer, and a C (8 nm)/Ni (6 nm)/Pt (10 nm) trilayer. The relatively thin Pt layer was chosen to prevent the possible development of intrinsic film roughness during the film deposition, and the particular thicknesses of each layer were optimized to achieve the highest reflectivity at 0.5 deg. The layers were deposited onto glass substrates (Schott D263 glass, 40 mm × 20 mm in size) by a direct current (DC) magnetron sputtering technique using a dedicated sputtering system designed at the Institute of Precision Optical Engineering of Tongji University.[23,24] The thickness of the glass substrates was only 0.3 mm, corresponding to the thickness of the D263 glass shells in the EP telescope. High-purity argon (99.999%) was used as the working gas. The base pressure was 1×10^{-4} Pa, and the deposition was applied at an Ar pressure of 0.4 Pa. During the deposition process, samples moved across the deposition area, and the deposition time was controlled by the sample speed. The deposition rates of the Pt, Ni, and C films were ~0.24, 0.11, and 0.02 nm/s, respectively. Several samples of each type were prepared simultaneously in the same deposition run and their structures were identical. In addition, the samples were kept in a clean room after deposition, the presence of hydrocarbon adhesion layer on mirror surface will not influence the reflectivity in the working spectral region-based our previous study.[25]

Grazing incidence x-ray reflectivity (GIXR) measurements were performed at the Cu-Kα emission line (photon energy $E = 8.04$ keV) using Bede D1[26,27] laboratory diffractometer. The angular step of measurements was 0.005 deg. The beam divergence of 0.007 deg is determined by the crystal [Si (220)] and the exit slit (100 μm) of monochromator. The measured GIXR curves (symbols) of the single-layer, bilayer, and trilayer coatings are shown in Fig. 6. The measured curves were normalized to the direct x-ray beam intensity (~1×10^5 counts per

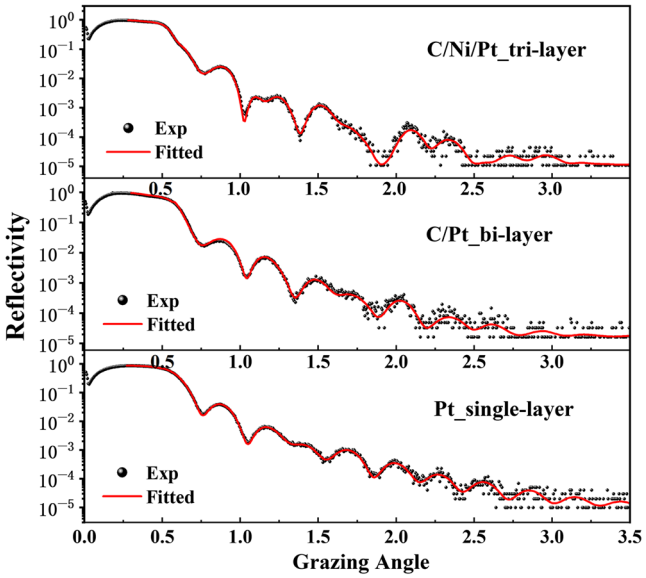

Fig. 6 Measured reflectivity (symbols) of Pt, C/Pt, and C/Ni/Pt samples versus the grazing incidence angle at a fixed photon energy of $E = 8.04$ keV. All curves are single reflection measurements and fitted results.

second after monochromatization and collimation) measured in the absence of sample. The red curves in Fig. 6 are the results of fitting performed with the use of Bede software based on the genetic algorithm.[27] The fitting parameters included the layer thicknesses, the material densities, and the interface widths characterizing the cumulative effect of the interlayers and small-scale (high-frequency) interface roughness.[13] The optical constants of materials were calculated based on their density and the atomic scattering factors of chemical elements taken from the CXRO database.[12]

The found values of the fitting parameters are listed in Table 1, where the material densities are presented as percentages of the bulk densities (2.2, 8.9, and 21.45 g/cm^3 for C, Ni, and Pt, respectively). The found thicknesses of all layers are very close to the desirable values indicated above. The material densities are close to the bulk ones. The interface width is almost the same for all the samples. We estimated roughly the errors in the found values of the parameters, which are also shown in Table 1. The indicated errors are maximal ones still keeping the calculated reflectivity curves within the interval of random oscillations on the experimental reflectivity curves shown in Fig. 6. Notice that the relatively large errors do not mean large errors of the reflectivity measurements, but weak influence of the parameters variation on the reflectivity of our samples. Indeed, Figs. 3(a) and 5 demonstrate that even 3 nm variation in the thickness of C or Ni layers results only in a modest change of the reflectivity curve shape. The similar conclusion can be done for the interface width, because our approach is based on the TER effect and

Table 1 Physical parameters of the studied reflective coatings as determined by fitting the measured GIXR curves.

Sample type	Material	Thickness (nm)	Interface width (nm)	Density (%)
Single layer	Pt	10.0 ± 0.5	0.37 ± 0.1	99 ± 2
Bilayer	C	8.0 ± 0.5	0.37 ± 0.1	97 ± 5
	Pt	10.0 ± 0.5	0.37 ± 0.1	99 ± 2
Trilayer	C	8.0 ± 0.5	0.37 ± 0.1	97 ± 2
	Ni	6.1 ± 0.8	0.36 ± 0.1	100 ± 2
	Pt	10.0 ± 0.5	0.35 ± 0.1	99 ± 5

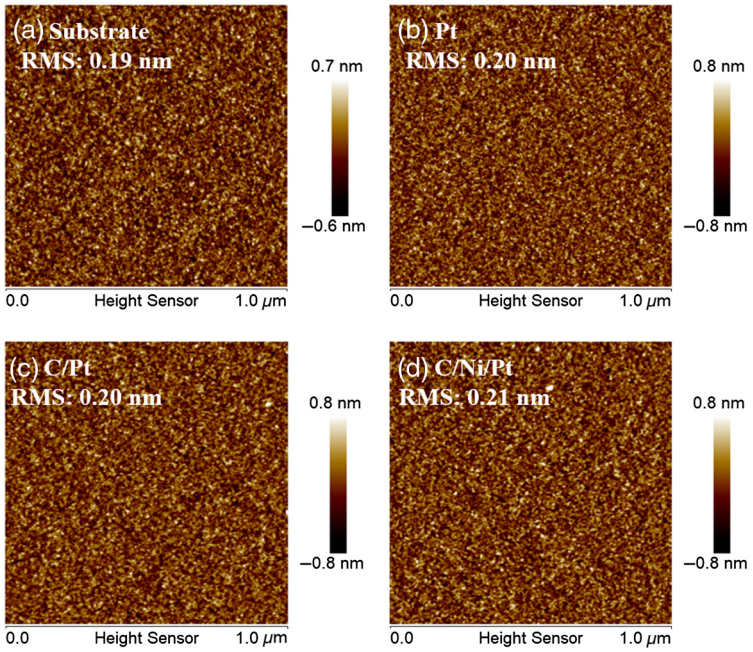

Fig. 7 AFM images of the external surface of (a) D263 glass substrate, (b) Pt single-layer, (c) C/Pt bi-layer, and (d) C/Ni/Pt trilayer samples. The surface microstructure was almost the same for all the samples.

the mirrors operate at small grazing angles, when the influence of interlayers on the reflectivity is very weak. Finally, a decrease in the density of materials by several percent will only result in proportional decrease in the width of the reflectivity plateau.

In addition, the external surfaces of the samples were studied using atomic force microscopy (AFM, Atomic Force Microscope, 1 μm × 1 μm scan size), and the AFM images are shown in Fig. 7. The root-mean-square (RMS) roughness was found to be practically the same (0.20 to 0.21 nm) for all the samples, qualitatively confirming the conclusions of the GIXR analysis. Furthermore, the roughness of the coated samples was almost the same as that of the bare substrate (0.19 nm). The error in the RMS roughness value was ± 0.005 nm, which was determined through AFM measurements of different areas on the sample surface.

Next, we determined the internal stress of the samples using a standard approach described below. Stress analysis is extremely important for telescope mirrors because a large stress will result in the deformation of thin substrates and will thus degrade the resolution of the telescope.[28]

Circular glass substrates measuring 30-mm in diameter and 1-mm in thickness were used for the fabrication of samples intended for the internal stress analysis. The sample curvature was measured using a Fizeau interferometer before and after coating deposition, and the stress was calculated using the Stoney equation. [29,30] The measured stress values for the single-layer, bilayer, and trilayer coatings are presented in Table 2. The samples exhibit a compressive stress of approximately the same absolute value. The main contribution to the intrinsic stress was introduced by the Pt film. Notice that the measured stress of Pt-based coatings is low compared to that of magnetron-deposited Ir films (of the order of GPa) studied in Ref. 31 and often used as reflecting coating in x-ray telescopes. Therefore, according to the estimations performed in Ref. 32, we conclude that the Pt-based samples exhibiting about −500 MPa internal stresses can be used in telescopes for the eXTP and EP missions characterizing by a relatively low angular resolution (∼60 arc sec). The application of C/Ni/Pt trilayer coatings in a telescope with a higher resolution

Table 2 Measured internal stress of the studied samples.

Sample type	Pt single layer	C/Pt bilayer	C/Ni/Pt trilayer
Stress (MPa)	-461 ± 62	-472 ± 51	-546 ± 54

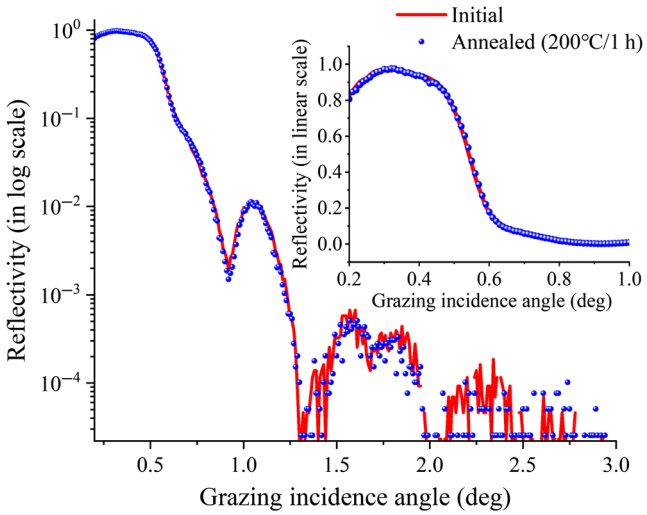

Fig. 8 Reflectivity of a C/Ni/Pt trilayer sample versus the grazing incidence angle before and after annealing in vacuum during 1 h at a temperature of 200°C. Inset: the reflectivity at small grazing incidence angle in the linear scale.

will require decreasing the internal stress, what can be achieved through the use of stress relaxation methods.[33,34]

Thermal stability is one of the more important parameters of a reflective coating.[35] The C/Ni/Pt trilayer sample was annealed in vacuum for 1 h at a temperature of 200°C. The GIXR measurements of the sample conducted before and after annealing resulted in identical reflectivity curves (Fig. 8), thus demonstrating the high thermal stability of the sample.

X-ray reflectivity measurements over a wide spectral interval were conducted at the KMC-1 beamline of the BESSY-II synchrotron.[36] The beamline covers a photon energy range of 2.1 to 10 keV. Figure 10 shows the reflectivity of the studied samples against the grazing incidence angle at a fixed photon energy of $E = 2.6$ keV (symbols). For comparison, the solid curves show the results of the calculations conducted with the sample parameters presented in Table 1 that were determined by fitting, using the simplest model, the experimental reflectivity curves measured using a laboratory diffractometer at $E = 8.04$ keV. The calculated curves and the experimental data match very well, as shown in Fig. 9. Very good agreement between the calculated

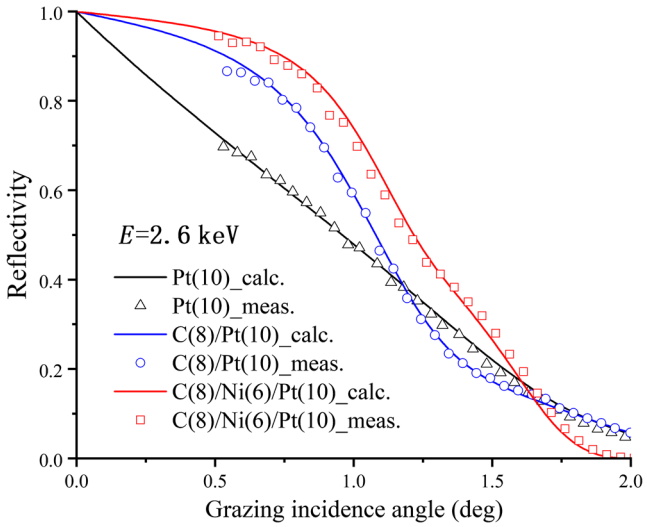

Fig. 9 Measured reflectivity (symbols) of the studied samples versus the grazing incidence angle at a photon energy of 2.6 keV. The solid curves were calculated using the layer parameters shown in Table 1.

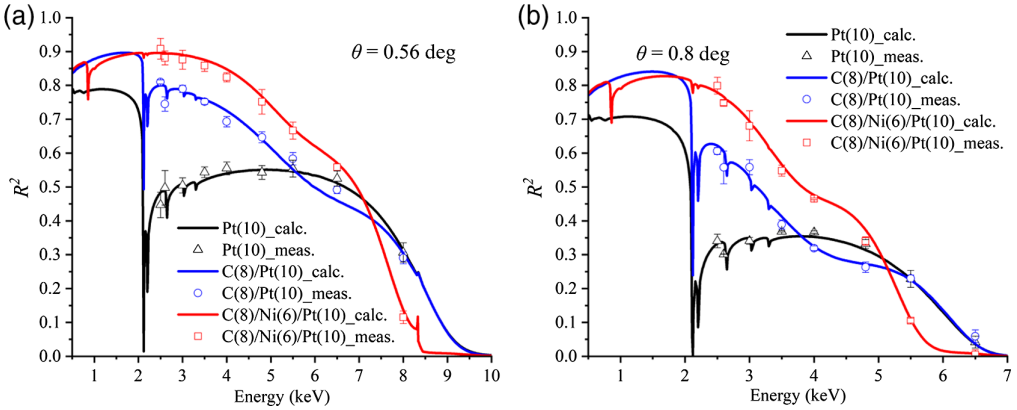

Fig. 10 Measured (symbols) and calculated (solid curves) double reflection coefficient of three studied samples versus the photon energy at a fixed grazing incidence angle of (a) $\theta = 0.56$ deg and (b) $\theta = 0.8$ deg. The calculations were conducted using the sample parameters presented in Table 1.

curves and the experimental data in Fig. 9 confirms the correctness of the determined parameters and the validity of the simplest model of the samples, which can thus be applied to predict the reflectivity of the samples in a wide range of photon energies and grazing incident angles.

The measured double reflection coefficient (symbols) of the studied samples against the photon energy for a fixed grazing incidence angle θ of 0.56 deg and 0.8 deg is plotted in Fig. 10. For comparison with the results of the theoretical analysis described in the previous section, the calculated double reflection coefficient R^2 is also shown in Fig. 10. The solid curves demonstrate the results of the calculations using the sample parameters listed in Table 1. A good agreement between the experimental data and theoretical predictions can be clearly seen in Fig. 10. Thus the conclusions regarding the theoretical analysis described in the previous section are confirmed by the experimental results. The double reflection coefficient R^2 of the C/Ni/Pt trilayer mirror largely exceeds that of the mirror coated by a single Pt layer. In particular, the reflectivity enhancement at $E = 2.6$ keV reaches a factor of 2 at $\theta = 0.56$ deg and 2.6 at $\theta = 0.8$ deg.

4 Conclusions

A comparative study of single layer, bilayer, and trilayer reflective coatings was conducted, aiming at improving the reflectivity of grazing incidence mirrors within the 0.5- to 8-keV energy region for the newly proposed Chinese space missions. A single layer of a high-Z material (Ir, Pt, and Au) is typically used as a reflective coating of mirrors in x-ray telescopes and synchrotron radiation beamlines. However, the M-edge of absorption of high-Z materials at $E \sim 2$ keV results in a low minimum value in the reflectivity curve and relatively low reflectivity (~50% to 60% after double reflection) above the absorption edge. Deposition of a low-Z material (C, B_4C) onto a heavy material layer allows masking the absorption edge and essentially increasing the reflectivity at low photon energies ($E < 3$ to 4 keV). Deposition of a medium-Z material (Co, Ni, and Cu) between heavy and light films provides a further increase in the reflectivity over the entire operation interval owing to the lower absorptivity of the intermediate layer and the larger polarizability. In particular, a C/Ni/Pt trilayer mirror allows an enhancement of the double reflection coefficient by a factor of 1.5 to 3.5 in the 2- to 4-keV energy range for a grazing incidence angle of $\theta = 0.5$ to 0.9 deg as compared to a mirror coated with a single Pt layer. As a result, the effective area of the telescope described in Ref. 22 is increased by a factor of 1.5 to 2.5 within the 2- to 4-keV range for the same telescope geometry.

For the experimental study, three samples were fabricated using a DC magnetron sputtering technique. Grazing incidence x-ray reflectometry was used to demonstrate the high quality of the samples. The measured layer thicknesses were extremely close to the thickness values chosen based on theoretical calculations, the material densities nearly coincided with those of the bulk material, and the interface width of ~0.37 nm was the same for all deposited layers.

AFM measurements (using a 1 μm $\times$ 1 μm scan size) of the three samples were also used to characterize the microstructure of the surface. It was found that the RMS roughness changed little: from 0.19 nm for an uncoated substrate to 0.21 nm for the trilayer C/Ni/Pt coating. The intrinsic stress was found to be relatively low, changing from −460 MPa (single Pt layer coating) to −540 MPa (trilayer C/Ni/Pt coating). Annealing the C/Ni/Pt trilayer mirror in vacuum for 1 h at 200°C did not change the GIXR reflectivity curve, demonstrating the high thermal stability of the sample. Reflectivity measurements in a wide spectral range were conducted at the BESSY-II synchrotron. The experimental results confirmed the conclusions obtained using the theoretical analysis. The double reflection coefficient of the C/Ni/Pt trilayer mirror was demonstrated to largely exceed that of the mirror coated by a single Pt layer. In particular, the double reflection coefficient at $E = 2.6$ keV was enhanced by a factor of 2 at a grazing angle $\theta = 0.56$ deg and 2.6 at $\theta = 0.8$ deg.

Acknowledgments

This work was supported by the National Natural Science Foundation of China (Nos. U1731242 and 61621001), Shanghai Rising-Star Program (No. 19QA1409200), and Shanghai Municipal Science and Technology Major Project (No. 2017SHZDZX02). One of the authors (I. V. K.) acknowledges the Russian Ministry of Science and Higher Education for the support of this work within the State Assignment FSRC "Crystallography and Photonic" RAS. Major projects of Science and Technology Commission of Shanghai (No. 17JC1400800).

References

1. P. Gorenstein, "Grazing incidence telescopes for x-ray astronomy," *Opt. Eng.* **51**(1), 011010 (2012).
2. K. Yamashita et al., "Supermirror hard-x-ray telescope," *Appl. Opt.* **37**(34), 8067–8073 (1998).
3. W. W. Zhang et al., "High-resolution, lightweight, and low-cost x-ray optics for the Lynx observatory," *J. Astron. Telesc. Instrum. Syst.* **5**(2), 021012 (2019).
4. M. C. Weisskopf, "Chandra x-ray optics," *Opt. Eng.* **51**(1), 011013 (2012).
5. J. W. den Herder et al., "The reflection grating spectrometer on board XMM-Newton," *Astron. Astrophys.* **365**(1), L7–L17 (2001).
6. J. E. Koglina et al., "NuSTAR hard X-ray optics," *Proc. SPIE* **5900**, 59000X (2005).
7. G. Sironi et al., "Simulating the optical performances of the ATHENA X-ray telescope optics," *Proc. SPIE* **10699**, 106993N (2018).
8. W. Yuan et al., "Einstein Probe—a small mission to monitor and explore the dynamic X-ray Universe," *Huazhong Univ. Sci. Technol. J.* **23**(4), 383 (2015).
9. W. Yuan et al., "Exploring the dynamic X-ray universe: Scientific opportunities for the Einstein Probe mission," *Chin. J. Space Sci.* **36**(2), 117–138, (2016).
10. S. Zhang et al., "The Enhanced X-ray Timing and Polarimetry mission—eXTP," *Sci. China: Phys. Mech. Astron.* **62**(2), 11433 (2018).
11. D. H. Lumb et al., "X-ray Multi-mirror Mission (XMM-Newton) observatory," *Opt. Eng.* **51**(1), 011009 (2012).
12. E. Gullikson, "Index of refraction," http://henke.lbl.gov/optical_constants/ (2010).
13. E. Spiller, *Soft X-Ray Optics*, SPIE Press, Bellingham, Washington (1994).
14. G. Pareschi et al., "Astronomical soft x-ray mirrors reflectivity enhancement by multilayer coatings with carbon overcoating," *Proc. SPIE* **5488**, 1–11 (2004).
15. D. Spiga et al., "Development of multilayer coatings (Ni/C-Pt/C) for hard x-ray telescopes by e-beam evaporation with ion assistance," *Proc. SPIE* **5488**, 813–819 (2004).
16. D. H. Lumb et al., "Influence of a carbon over-coat on the X-ray reflectance of XEUS mirrors," *Optics Communications* **279**(1), 101–105 (2007).
17. N. J. Westergaard, et al., "On X-ray telescopes in general and the Athena optics in particular," *Nucl. Instr. Meth. A* **873**(21), 5–11, (2017).
18. D. E. Graessle et al., "Molecular contamination study of iridium-coated x-ray mirrors," *Proc. SPIE* **2279**, 12–26 (1994).

19. Y. Ogasaka et al., "Application of composite-layer mirror to soft x-ray telescopes," *Proc. SPIE* **5488**, 849–855 (2004).
20. K. Mech et al., "Cu thin films deposited by DC magnetron sputtering for contact surfaces on electronic components," *Arch. Metall. Mater.* **56**(4), 903–908 (2011).
21. V. E. Asadchikov et al., "Sliced zone plate for hard X-ray sources. Manufacturing and testing," *Proc. SPIE* **3113**, 384–392 (1997).
22. Y. Liao et al., "Optical design and simulations of the soft x-ray telescope for Einstein Probe mission," *Proc. SPIE* **10399**, 103990L (2017).
23. R. Qi et al., "Effects of sputtering parameters and separator plates on the structure and stress of W/Si multilayers in x-ray telescope applications," *Opt. Eng.* **56**(3), 035103 (2017).
24. Z. Wang et al., "Development of imaging x-ray telescopes at Tongji University," *J. Astron. Telesc. Instrum. Syst.* **5**(4), 044010 (2019).
25. L. Jiang et al., "Investigation of natural contamination layer growth on optical substrates," *Chin. Phys. C*, **42**(11), 115001 (2018).
26. D. K. Bowen and R. D. Deslattes, "X-ray metrology by diffraction and reflectivity," *Proc. AIP* **550**(550), 570–579 (2001).
27. M. Wormington et al., "Characterization of structures from X-Ray scattering data using genetic algorithms," *Philos. Trans.: Math. Phys. Eng. Sci.* **357**(1761), 2827–2848 (1999).
28. H. Mori et al., "Reflective coatings for the future x-ray mirror substrates," *Proc. SPIE* **10699**, 1069941 (2018).
29. M. R. Ardigo et al., "Stoney formula: investigation of curvature measurements by optical profilometer," *Adv. Mater. Res.* **996**, 361–366 (2014).
30. Q. Huang et al., "Structure and stress studies of low temperature annealed W/Si multilayers for the X-ray telescope," *Opt. Express* **24**(14), 15620–15630 (2016).
31. K. Chan et al., "Reflective coatings for lightweight X-ray optics," *Proc. SPIE* **8443**, 84433S (2012).
32. F. Christensen et al., "Coatings for the NuSTAR mission," *Proc. SPIE* **8147**, 81470U (2011).
33. Y. Yao et al., "Progress of coating stress compensation of silicon mirrors for Lynx x-ray telescope mission concept using thermal oxide patterning method," *J. Astron. Telesc. Instrum. Syst.* **5**(2), 021011 (2019).
34. A. Probst et al., "Coating stress analysis and compensation for iridium based X-ray mirrors," *Appl. Opt.* **57**(29), 8775–8779 (2018).
35. D. M. Ferreira et al., "Design, development, and performance of x-ray mirror coatings for the ATHENA mission," *Proc. SPIE* **10399**, 1039918 (2017).
36. F. Schäfers et al., "KMC-1: a high resolution and high flux soft X-ray beamline at bessy," *Rev. Sci. Instrum.* **78**(12), 123102 (2007).

Zhanshan Wang received his MS degree in optics from Changchun Institute of Optics and Fine Mechanics of Chinese Academy of Sciences (CAS) in 1988 and his PhD in optics from Shanghai Institute of Optics and Fine Mechanics of CAS in 1996. He is a SPIE fellow and a professor at Tongji University. He is the author of more than 150 journal papers. His current research interests include soft x-ray sources, optics in extreme ultraviolet and x-ray region, optical coatings for lasers, and optical systems.

Biographies of the other authors are not available.